

# FT3L core datasheet

## Grid Asset Performance > Next Generation Transformers

Hitachi FT-3TL core uses nanocrystalline soft magnetic material FINEMET® suitable for medium frequency transformers, especially in high-power applications. It contributes to downsize and improves efficiency in transformers. Low core loss and high saturation flux density for effective power transforming.

Date: June 2019  
Revision 0.2

© U.S. Department of Energy - National Energy Technology Laboratory



FT3L core

Fig. 1: Core under test.

## Dimensions

Table 1: Core dimensions.

Description	Symbol	Finished dimension (mm)
Width of core	A	180
Height of core	B	240
Depth of core (or cast width)	D	30
Thickness or build	E	50
Width of core window	F	80
Height of core window	G	140

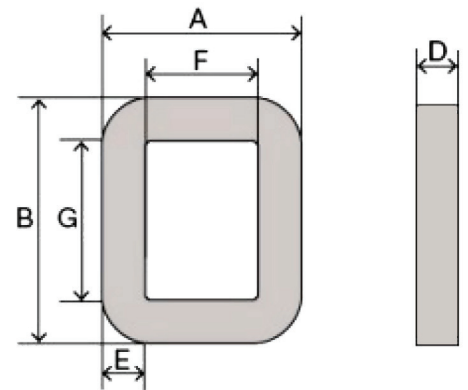


Fig. 2: Illustration of core dimensions.

## Acknowledgement

This technical effort was performed in support of the National Energy Technology Laboratory's ongoing research in DOE's The Office of Electricity's (OE) Transformer Resilience and Advanced Components (TRAC) program under the RSS contract 89243318CFE000003.

## Disclaimer

This work was funded by the Department of Energy, National Energy Technology Laboratory, an agency of the United States Government, through a support contract with Leidos Research Support Team (LRST). Neither the United States Government nor any agency thereof, nor any of their employees, nor LRTS, nor any of their employees, makes any warranty, expressed or implied, or assumes any legal liability or responsibility for the accuracy, completeness, or usefulness of any information, apparatus, product, or process disclosed, or represents that its use would not infringe privately owned rights. Reference herein to any specific commercial product, process, or service by trade name, trademark, manufacturer, or otherwise, does not necessarily constitute or imply its endorsement, recommendation, or favoring by the United States Government or any agency thereof. The views and opinions of authors expressed herein do not necessarily state or reflect those of the United States Government or any agency thereof.



## Magnetic Characteristics

Table 2: Core physical characteristics.

Description	Symbol	Typical value	Unit
Effective area	$A_e$	1,125	mm <sup>2</sup>
Mean magnetic path length	$L_m$	575	mm
Weight	<i>Weight</i>	4.7	kg
Permeance/inductance per turn	$A_L$	39.3 ( $\pm 30\%$ )	$\mu\text{H}/\text{N}^2$
Max core loss @ 0.1T	$P_C$	2.9	W
Saturation flux density	$B_{sat}$	1.2	T
Effective volume	$V_e$	646875	mm <sup>3</sup>
Core stacking factor	$k_f$	0.75	Dimensionless

## Measurement Setup

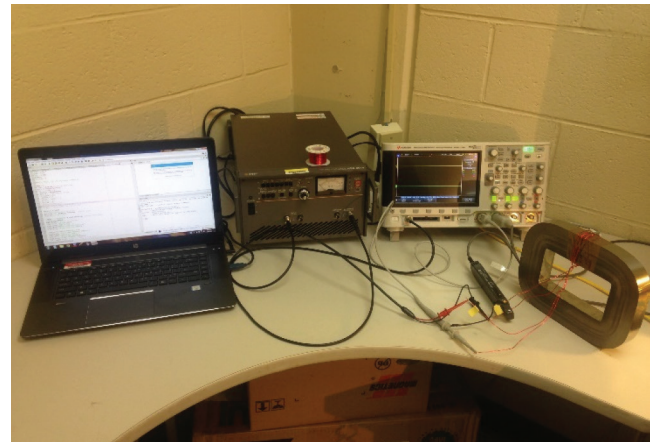
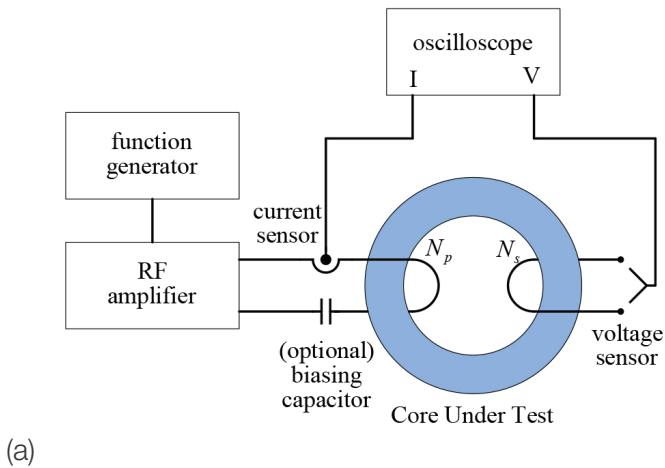


Fig. 3: Arbitrary waveform core loss test system (CLTS) (a) conceptual setup (b) actual setup.

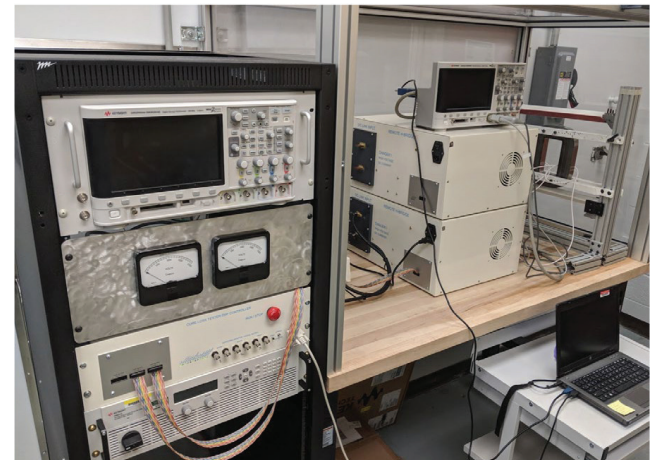
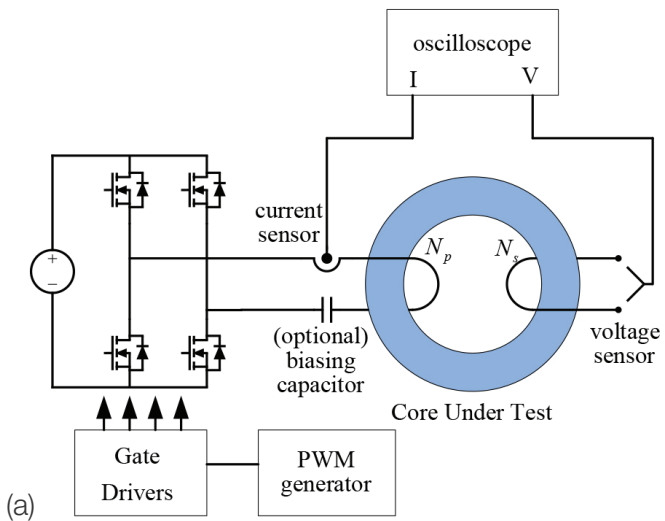


Fig. 4: Square waveform core loss test system (CLTS) (a) conceptual setup (b) actual setup.

Arbitrary and square waveform core loss test systems (CLTS) are utilized to characterize soft magnetic materials, which are shown in Fig. 3 and Fig. 4, respectively. Fig. 5 illustrates three different excitation voltage waveforms and corresponding flux density waveforms. In the arbitrary waveform CLTS, a function generator generates any arbitrary small signal, and the small signal is amplified and applied to a core under test (CUT) using a linear amplifier. The arbitrary waveform CLTS is advantageous in that any waveforms can be easily applied to characterize a CUT; however, the linear amplifier has limited electrical capabilities, such as  $\pm 75\text{V}$  &  $\pm 6\text{A}$  peak ratings and  $400\text{V}/\mu\text{s}$  slew rate. Therefore, a full core characterization may not be possible in some cases, such as low permeability cores, high frequency, and/or large sized cores. The arbitrary waveform CLTS is utilized to perform sinusoidal waveform measurements, as shown in Fig. 5(a). The square waveform CLTS is utilized to perform various square waveform measurements with different duty cycles, as shown in Fig. 5(b) and (c). 1200V SiC MOSFET devices are utilized to extend the core characterization range.

Two windings are placed around the core under test. The amplifier excites the primary winding, and the current of the primary winding is measured, in which the current information is converted to the magnetic field strengths  $H$  as

$$H(t) = \frac{N_p \cdot i(t)}{l_m}, \quad (1)$$

where  $N_p$  is the number of turns in the primary winding. A dc-biasing capacitor is inserted in series with the primary winding to provide zero average voltage applied to the primary winding.

The secondary winding is open, the voltage across the secondary winding is measured, in which the voltage information is integrated to derive the flux density  $B$  as

$$B(t) = \frac{1}{N_s \cdot A_e} \int_0^T v(\tau) d\tau, \quad (2)$$

where  $N_s$  is the number of turns in the secondary winding, and  $T$  is the period of the excitation waveform.

In Fig. 5(a), the excitation voltage is sinusoidal, and its flux waveform is also a sinusoidal shape. In Fig. 5(b), the excitation voltage is a two-level square waveform with asymmetrical duty cycle between high-level and low-level voltages, and its flux waveform is a sawtooth shape. It is hereafter referred as asymmetrical waveform. Its duty cycle is defined as the ratio between the applied high voltage time and the period, and the duty cycle can range from 0% to 100%. Furthermore, the average excitation voltage is adjusted to be zero via the dc-biasing capacitor, and thus, the average flux is also zero.

In Fig. 5 (c), the excitation voltage is a three-level square voltage with symmetrical duty cycle between high-level and low-level voltages, and its flux waveform is a trapezoidal shape. It is hereafter referred as symmetrical waveforms. Its duty cycle is defined as the ratio between the applied high-level voltage time and the period, and the duty cycle can range from 0% to 50%. At 50% duty cycles, both the asymmetrical and symmetrical waveforms become identical.

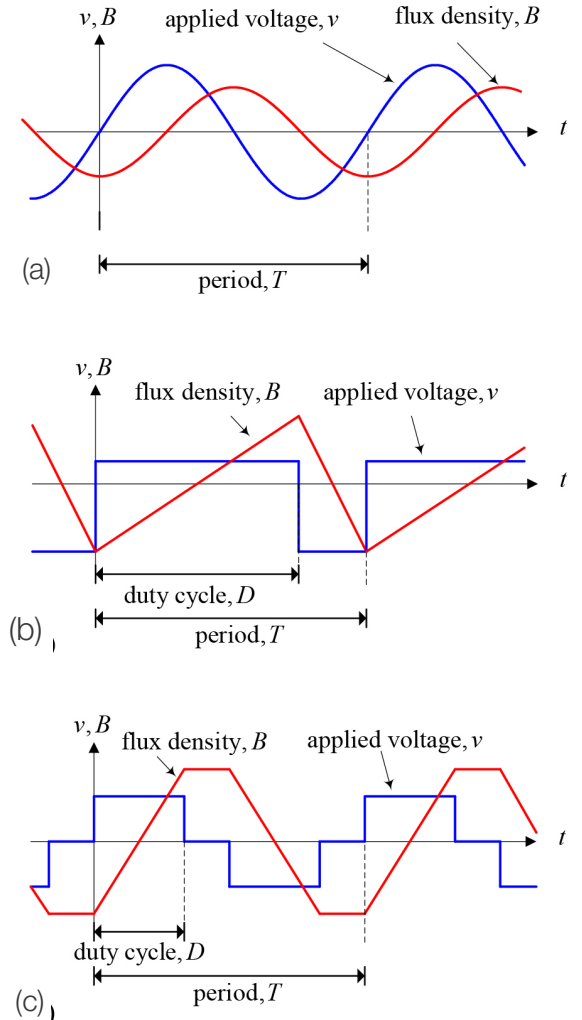


Fig. 5: Excitation voltage waveforms and corresponding flux density waveforms (a) Sinusoidal excitation with sinusoidal flux, (b) Asymmetrical excitation with sawtooth flux, and (c) Symmetrical excitation with trapezoidal flux.

## Core Losses

Core losses at various frequencies and induction levels are measured using various excitation waveforms. Based on measurements, the coefficients of the Steinmetz's equation are estimated. The Steinmetz's equation is given as

$$P_w = k_w \cdot (f / f_0)^\alpha \cdot (B / B_0)^\beta, \quad (3)$$

where  $P_w$  is the core loss per unit weight,  $f_0$  is the base frequency,  $B_0$  is the base flux density, and  $k_w$ ,  $\alpha$ , and  $\beta$  are the Steinmetz coefficients from empirical data. In the computation of  $P_w$ , the weight before impregnation in Table 2 is used, the base frequency  $f_0$  is 1 Hz, and the base flux density  $B_0$  is 1 Tesla.

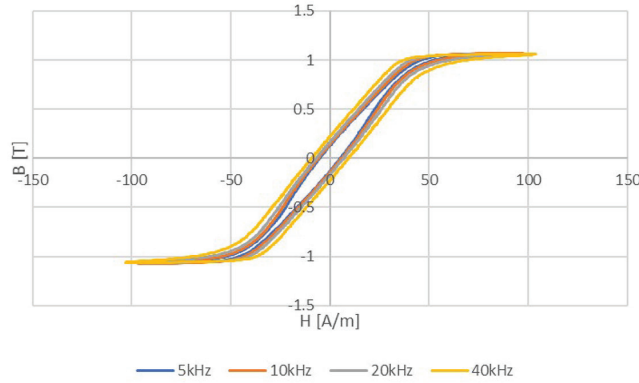


Fig. 6: BH curve as a function of frequency.

Fig. 6 illustrates the measured BH curve at different frequencies. The field strength  $H$  is kept near constant for all frequency. At 5 kHz and 10 kHz excitations, the BH curve is similar, which indicates that the hysteretic losses are the dominant factor at frequencies below 5 kHz. As frequency increases, the BH curves become thicker, which indicates that the eddy current and anomalous losses are becoming larger.

Table 3: Steinmetz coefficients.

	$k_w$	$A$	$\beta$
sine	4.60301004642584e-05	1.39468034842719	2.05765721687426
Square 50% duty	9.22817131405644e-06	1.57895862291895	2.96808224330713
Asymmetrical 40% duty	6.10034128104189e-06	1.62277870937581	3.06411897778253
Asymmetrical 30% duty	6.74575303677176e-06	1.62030628410133	2.95418655971996
Asymmetrical 20% duty	5.35936922374620e-06	1.65495143286460	2.71055284641337
Asymmetrical 10% duty	1.41102085911408e-05	1.57499569290072	2.12321581274459
Symmetrical 40% duty	1.11185976069850e-05	1.57758004535130	2.71321994937254
Symmetrical 30% duty	1.01910427135361e-05	1.60598858605388	2.64722227688454
Symmetrical 20% duty	1.85663584584057e-05	1.56469000170295	2.28989365330761
Symmetrical 10% duty	2.69835756686002e-05	1.56153699791516	2.09658336758682

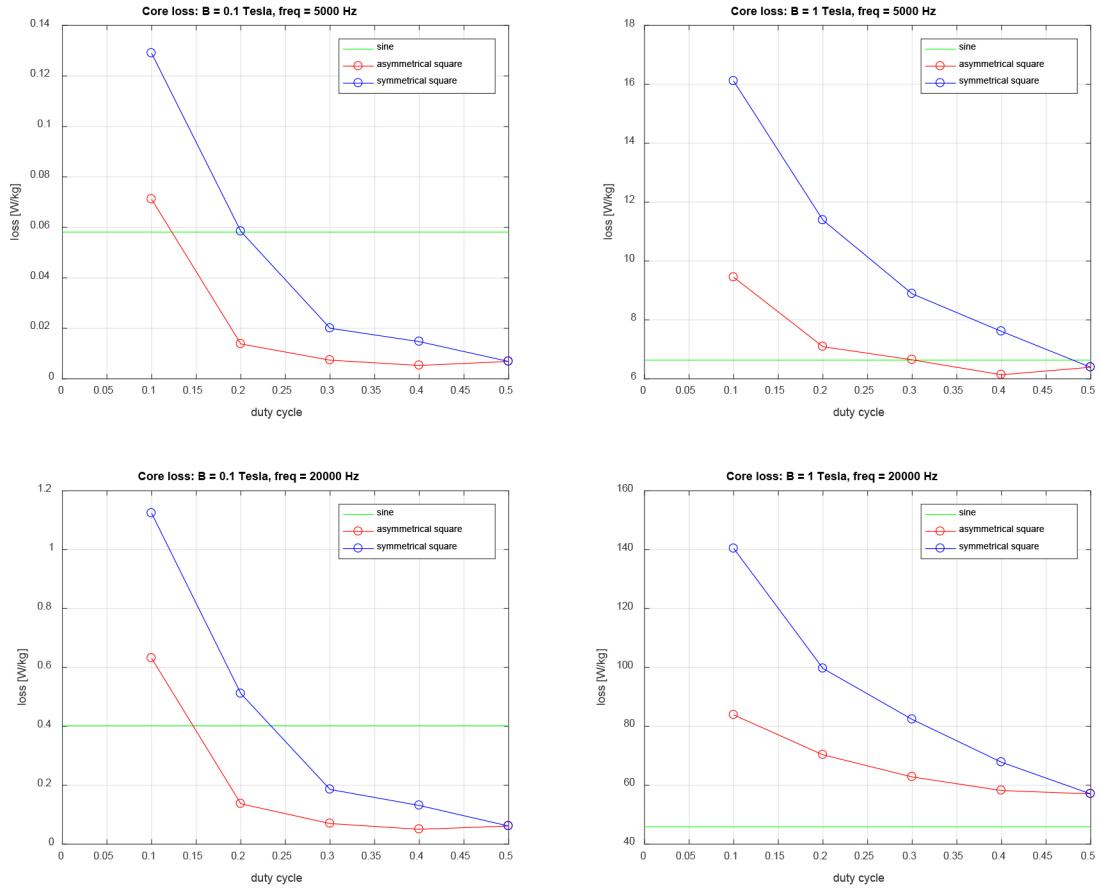


Fig. 7: Estimated core losses of sine and square excitation at various flux density, frequency, and duty cycle.

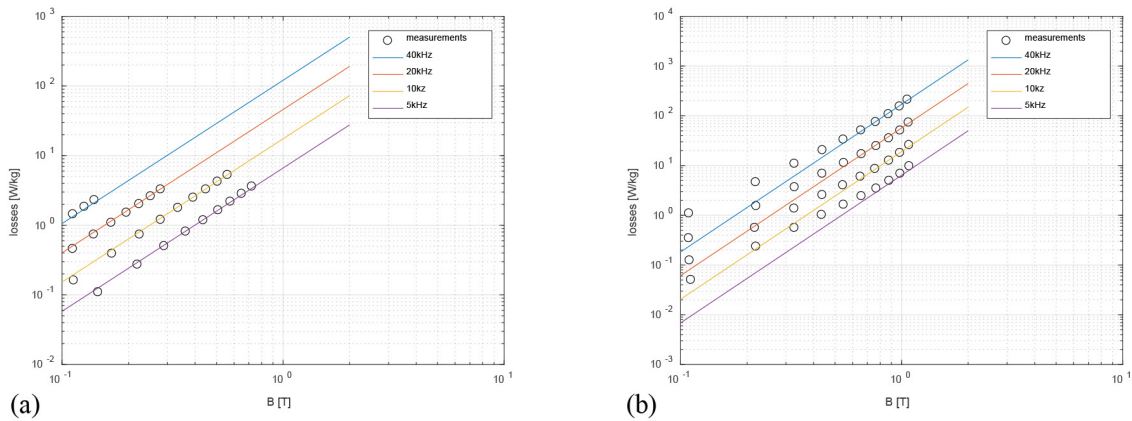


Fig. 8: Core loss measurements and estimations via Steinmetz equation: (a) Sine (b) Square at 50% duty.

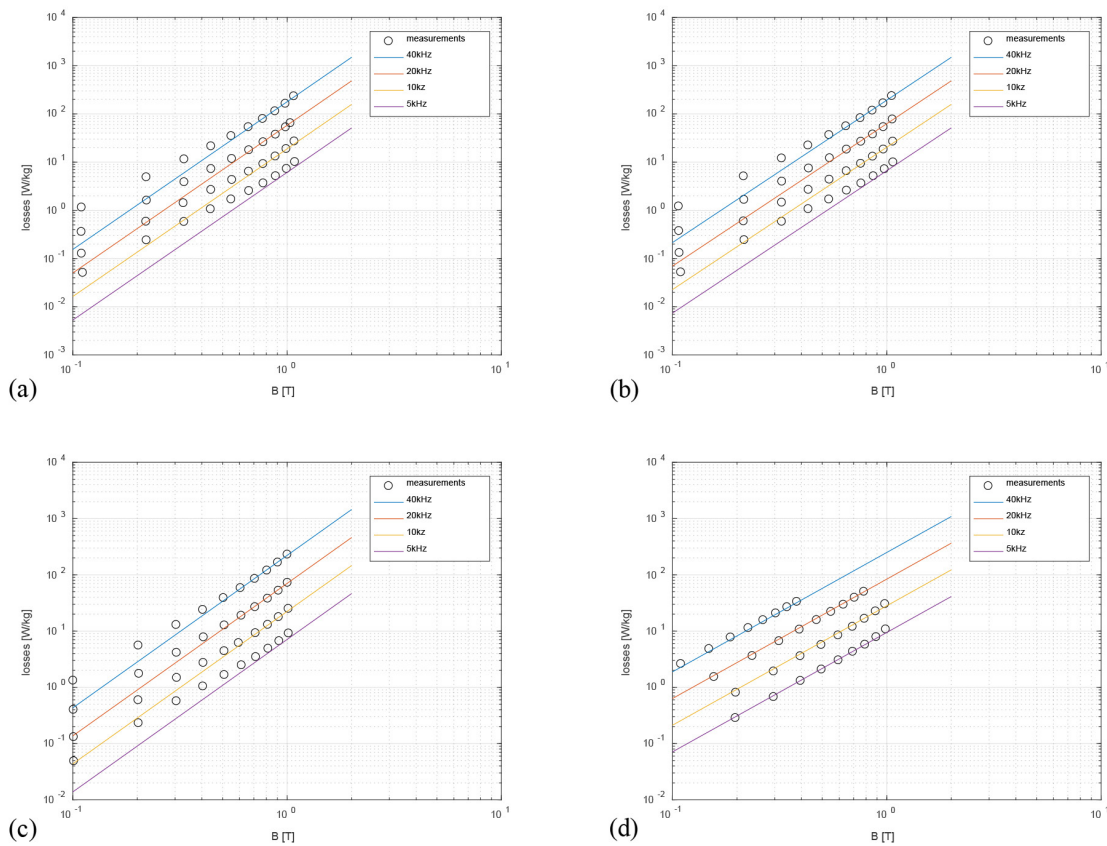


Fig. 9: Core loss measurements and estimations via Steinmetz equation of asymmetrical square waveform excitation: (a) 40% duty (b) 30% duty (c) 20% duty (d) 10% duty.

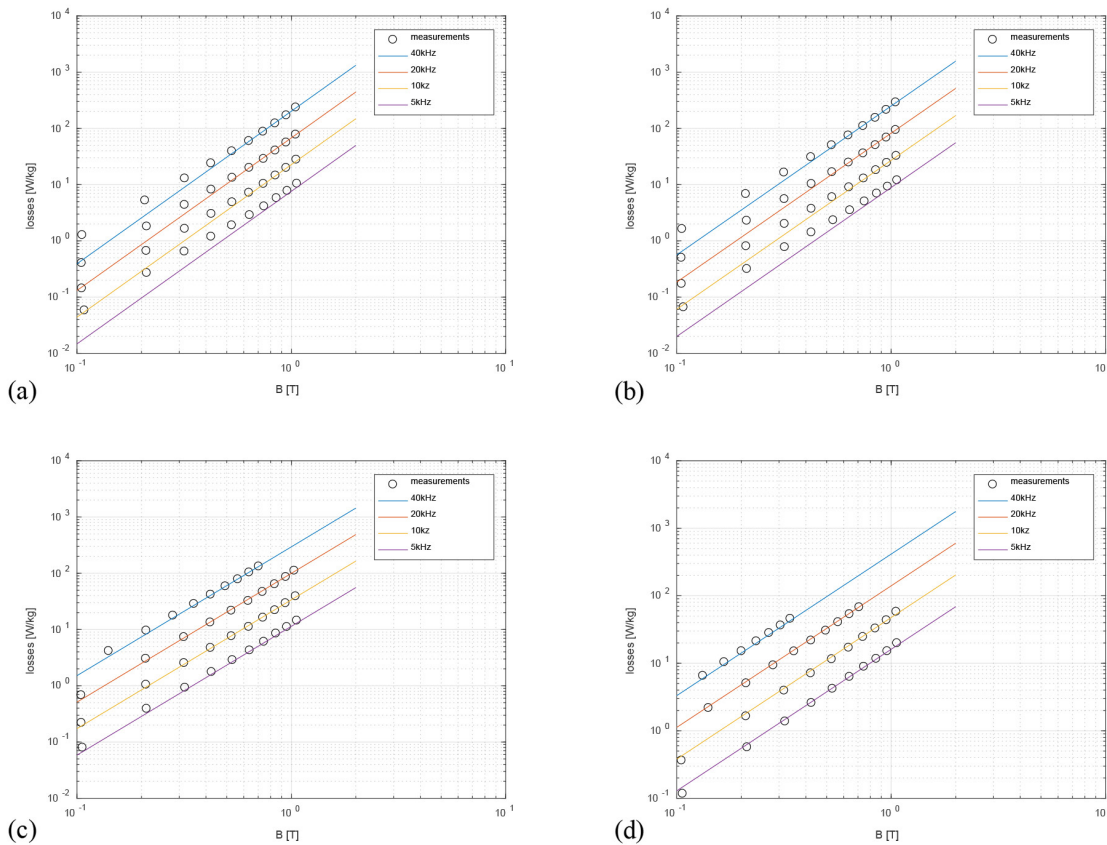


Fig. 10: Core loss measurements and estimations via Steinmetz equation of symmetrical square waveform excitation: (a) 40% duty (b) 30% duty (c) 20% duty (d) 10% duty.

## Core Permeability

The permeability of the core is measured as functions of flux density and frequency. Following figures illustrate the measured absolute relative permeability  $\mu_r$  values, which is defined as

$$\mu_r = \frac{B_{peak}}{\mu_0 \cdot H_{peak}} \quad (4)$$

where  $B_{peak}$  and  $H_{peak}$  are the maximum flux density and field strength at each measurement point. Under certain excitation conditions, the core could not be saturated due to lack of available voltages. For example, the sine excitation is performed using the arbitrary CLTS, and its voltage is limited to  $\pm 75V$ . Furthermore, the square CLTS could not saturate the core during the highest frequency and 10% duty cycle.

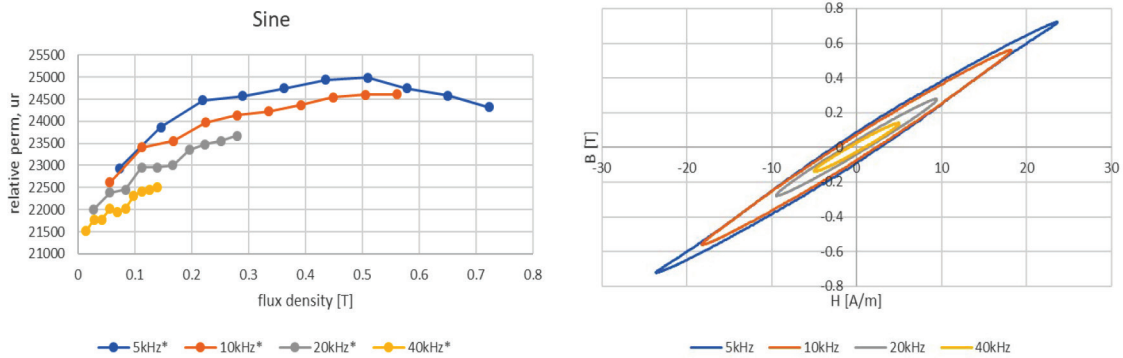


Fig. 11 Sinusoidal excitation: relative permeability as a function of flux density and frequency (left column) and BH loop at the maximum  $B$  of the corresponding frequency (right column) (\* could not saturate the core under the condition).

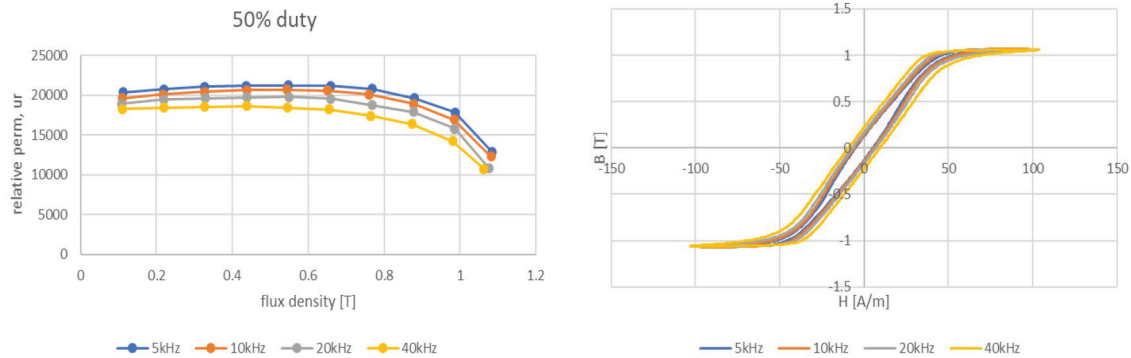


Fig. 12: Square excitation with 50% duty cycle: relative permeability as a function of flux density and frequency (left column) and BH loop at the maximum  $B$  of the corresponding frequency (right column).

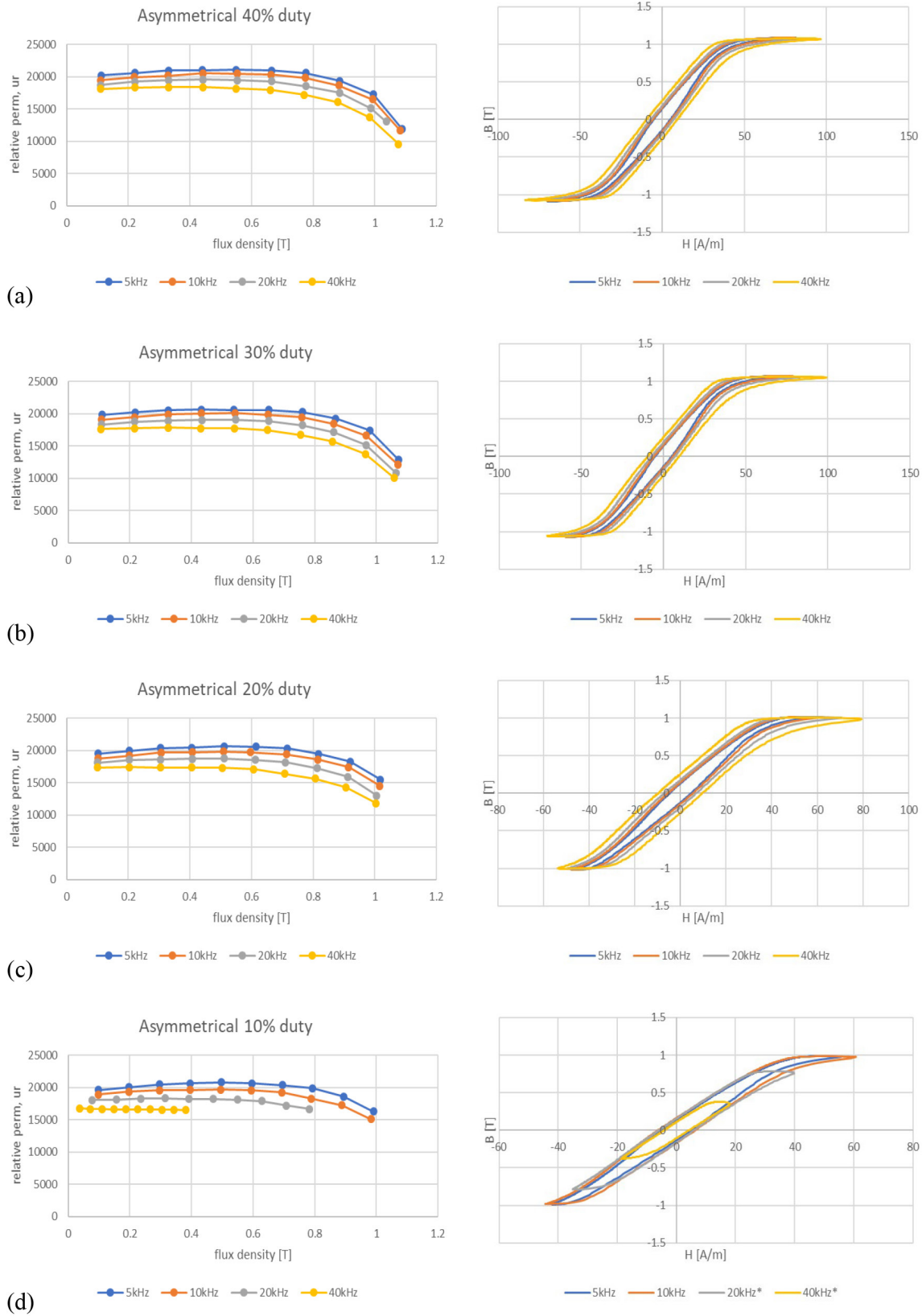


Fig. 13: Asymmetrical excitation with various duty cycle: relative permeability as a function of flux density and frequency (left column) and BH loop at the maximum B of the corresponding frequency (right column) (a) 40% duty (b) 30% duty (c) 20% duty (d) 10% duty (\* could not saturate the core under the condition).

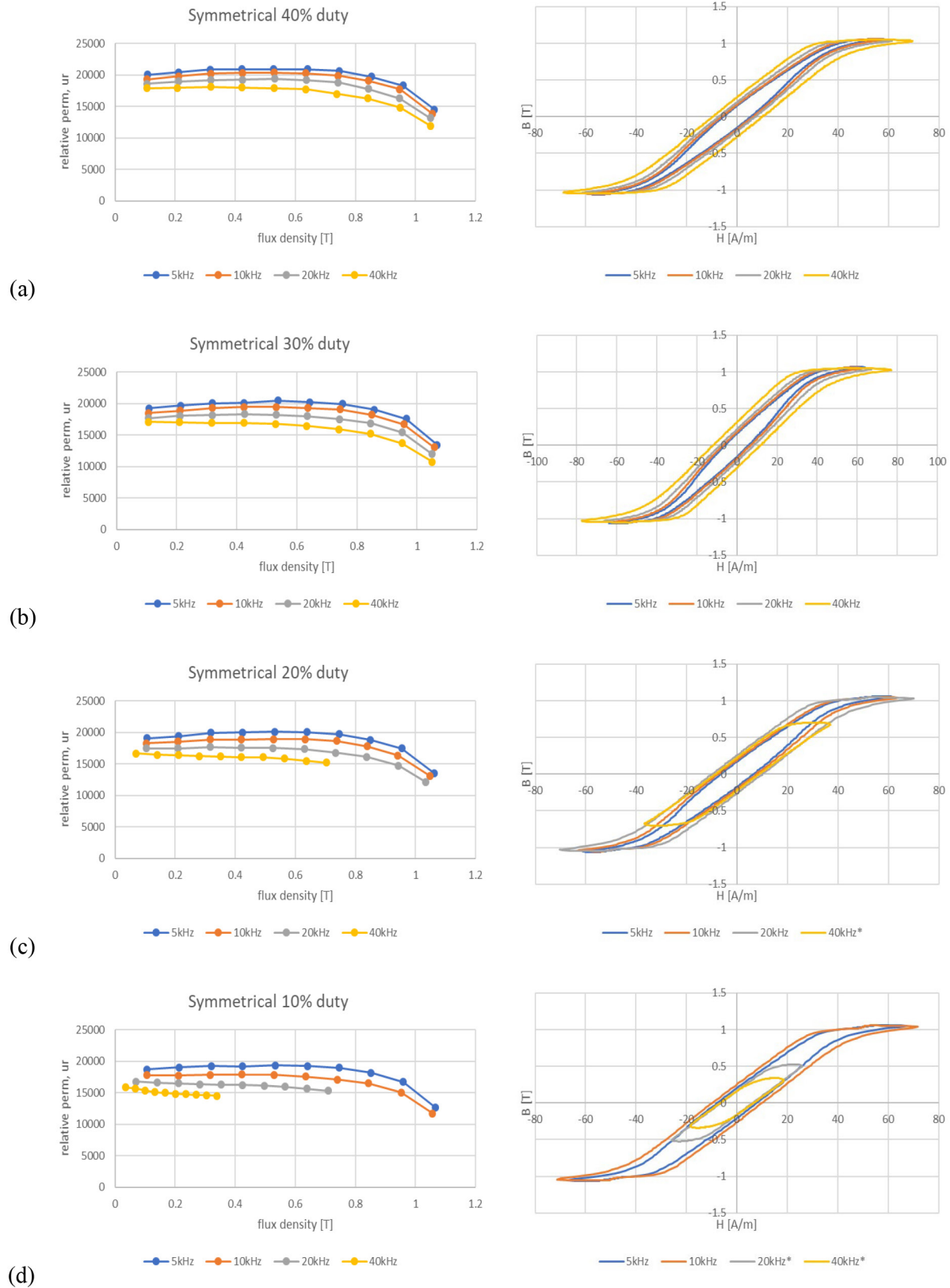


Fig. 14: Symmetrical excitation with various duty cycle: relative permeability as a function of flux density and frequency (left column) and BH loop at the maximum B of the corresponding frequency (right column) (a) 40% duty (b) 30% duty (c) 20% duty (d) 10% duty (\* could not saturate the core under the condition).

## Anhysteretic BH Curves

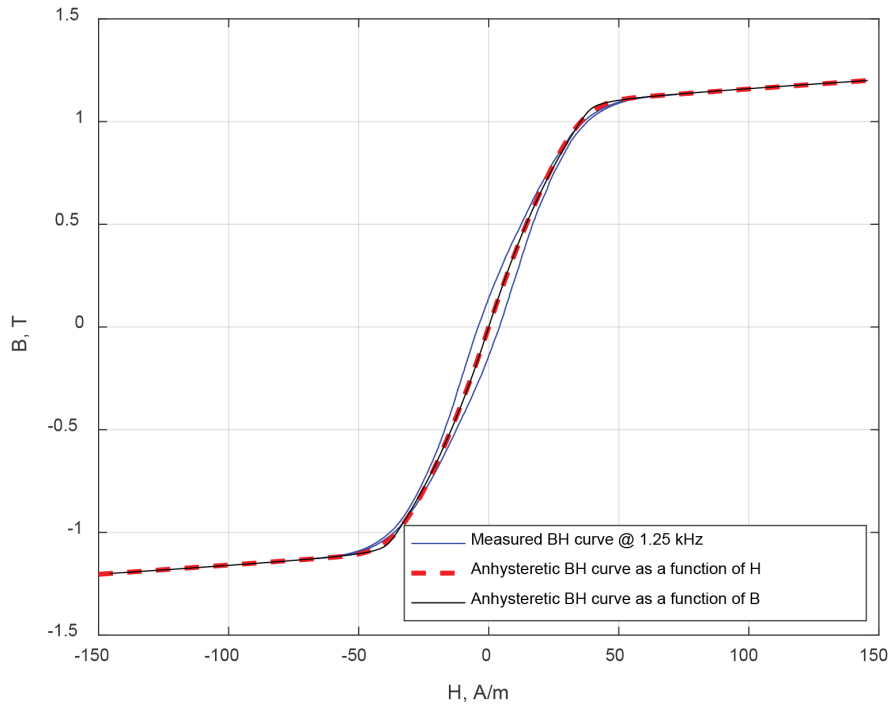


Fig. 15: Measured BH curve and fitted anhysteretic BH curve as functions of H and B

Table 4: Anhysteretic curve coefficients for B as a function of H.

$k$	1	2	3	4
$m_k$	1.56515767341055	-0.0351169534483996	0.661161875122230	0.353567458458664
$h_k$	74.9868505793837	34.0980241013168	63.1435618320739	45.1082360733275
$n_k$	1	4.99999984973286	2.54267243853586	4.83318459475986

Table 5: Anhysteretic curve coefficients for H as a function of B.

$k$	1	2	3	4
$\mu_r$	31643.8738416898			
$\alpha_k$	0.590171287250857	0.590171287250857	0.590171287250857	0.590171287250857
$\beta_k$	78.0469534287607	78.0469534287607	78.0469534287607	78.0469534287607
$\gamma_k$	1.56539814076458	1.56539814076458	1.56539814076458	1.56539814076458
$\delta_k$	0.00756174663229553	0.00756174663229553	0.00756174663229553	0.00756174663229553
$\varepsilon_k$	8.71494381444516e-54	8.71494381444516e-54	8.71494381444516e-54	8.71494381444516e-54
$\zeta_k$	1	1	1	1

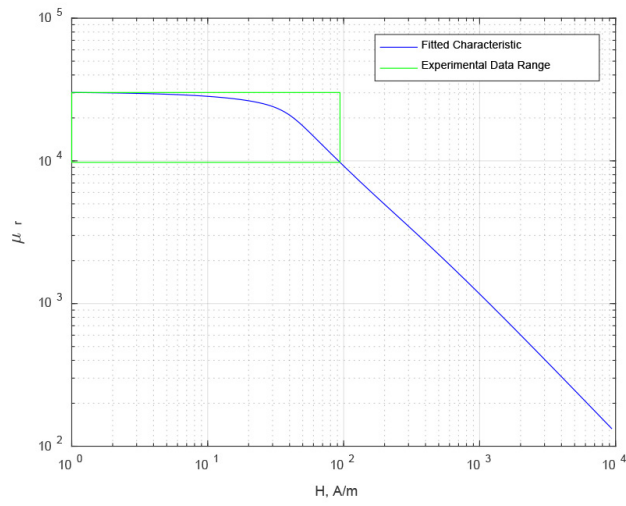


Fig. 16: Absolute relative permeability as function of field strength  $H$ .

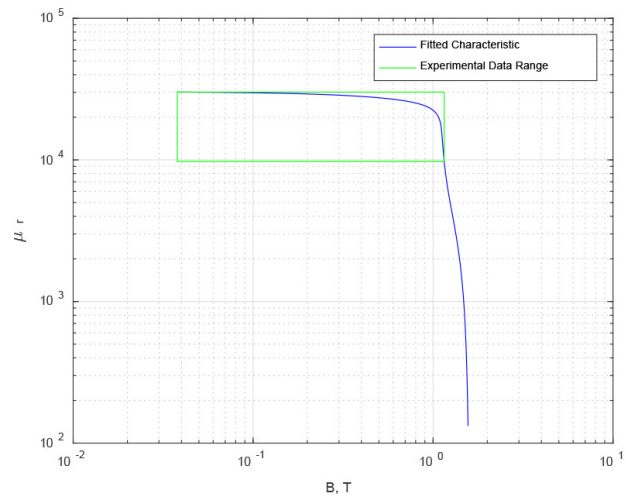


Fig. 17: Absolute relative permeability as function of flux density  $B$ .

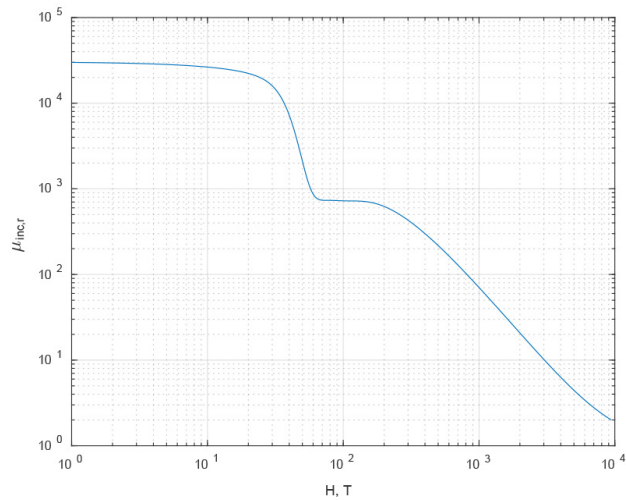


Fig. 18: Incremental relative permeability.

Fig. 15 illustrates the measured low frequency BH loops at 100 Hz. Using the outer most BH loop, the anhysteretic BH curve is fitted. The anhysteretic BH curves can be computed as a function of field intensity H using the follow formula.

$$B = \mu_H (H) H$$

$$\mu_H (H) = \mu_0 + \sum_{k=1}^K \frac{m_k}{h_k} \frac{1}{1 + |H / h_k|^{n_k}} \quad (5)$$

Similarly, the anhysteretic BH curves can be computed as a function of flux density B using the follow formula.

$$B = \mu_B (B) H$$

$$\mu_B (B) = \mu_0 \frac{r(B)}{r(B) - 1}$$

$$r(B) = \frac{\mu_r}{\mu_r - 1} + \sum_{k=1}^K \alpha_k |B| + \delta_k \ln(\varepsilon_k + \zeta_k e^{-\beta_k |B|}) \quad (6)$$

$$\delta_k = \frac{\alpha_k}{\beta_k}, \varepsilon_k = \frac{e^{-\beta_k \gamma_k}}{1 + e^{-\beta_k \gamma_k}}, \zeta_k = \frac{1}{1 + e^{-\beta_k \gamma_k}}$$

Table 4 and Table 5 lists the anhysteretic curve coefficients for eqs. (5) and (6), respectively.

The core anhysteretic characteristic models in eqs. (5) and (6) are based on the following references.

Scott D. Sudhoff, "Magnetics and Magnetic Equivalent Circuits," in *Power Magnetic Devices: A Multi-Objective Design Approach*, 1, Wiley-IEEE Press, 2014, pp.488-

G. M. Shane and S. D. Sudhoff, "Refinements in Anhysteretic Characterization and Permeability Modeling," in *IEEE Transactions on Magnetics*, vol. 46, no. 11, pp. 3834-3843, Nov. 2010.

The estimation of the anhysteretic characteristic is performed using a genetic optimization program, which can be found in the following websites:

[https://engineering.purdue.edu/ECE/Research/Areas/PEDS/go\\_system\\_engineering\\_toolbox](https://engineering.purdue.edu/ECE/Research/Areas/PEDS/go_system_engineering_toolbox)

## Core Characteristic Variation as a Function of Temperature

At this time, the core temperature is not monitored, and this version of data sheet does not have this information. However, in future editions, it is planned to be included.